Constraints from fault roughness on the scale-dependent strength of rocks

Emily E. Brodsky[1], James D. Kirkpatrick[2] and Thibault Candela[1]
[1]Department of Earth and Planetary Sciences, University of California–Santa Cruz, 1156 High Street, Santa Cruz, California 95064, USA
[2]Department of Earth and Planetary Sciences, McGill University, 3450 University Avenue, Montreal, Quebec H3A 0E8, Canada

ABSTRACT

Principal slip surfaces in faults have measurable roughness generated during slip. The roughness both records previous events and poses the boundary conditions for future rupture. Digital, high-precision roughness data are now available at the field scale (tens of centimeters to tens of meters) for at least 22 faults, and at the laboratory scale (millimeters to tens of centimeters) for a subset of these. We quantify the slip surface roughness by measuring the aspect ratio, which is the average asperity height divided by the profile length. Higher aspect ratios indicate rougher surfaces. From the field studies, two major trends have emerged: (1) fault surface roughness lies in a restricted range with aspect ratios in the slip-parallel direction of 0.07%–0.5% for profiles of 1 m length, and (2) fault surfaces are rougher at small scales than large ones. These features can both be interpreted as fingerprints of scale-dependent strength, which sets a limit to the aspect ratio of the surface. The measurements imply that shear strength scales with the observation scale, L, as $L^{-0.4}$. The new understanding of the physical controls on roughness allows generalization of the extant measurements of a wide array of faults.

INTRODUCTION

Fault zones contain well-defined slip surfaces. Field investigations of faults have long recognized striae, slickenlines, and grooving, indicating that each surface records mechanical wear during relative motion of opposing sides of the fault (Lyell, 1871). The direct imprint of wear distinguishes the slip surfaces as useful indicators of the mechanical processes operating during slip.

The geometry of the fault surfaces has been investigated both to constrain the boundary conditions of future slip and to examine the effects of previous ruptures. Measurement of the fault surface roughness initially relied on mechanical profilometers (Brown and Scholz, 1985; Power et al., 1988; Power and Tullis, 1991; Lee and Bruhn, 1996). These investigations confirmed that the smoothest profiles on faults are in the slip-parallel direction. Over the past decade, scanning with ground-based lidar and other optical scanning methods has enabled higher precision high-density measurements (Renard et al., 2006; Sagy et al., 2007; Bistacchi et al., 2011; Brodsky et al., 2011; Candela et al., 2012). The roughness of at least 22 faults has been measured (Table DR1 in the GSA Data Repository[1]).

Like other natural surfaces, faults have scale-dependent roughness. Fourier analysis provides an effective tool for analyzing the scale dependence. Fault roughness has therefore been studied by calculating spectra from profiles aligned with slip on the fault surface. For each fault, the topographic data are taken by either ground-based lidar on an exposure of the exhumed fault surface or a laboratory laser profilometer on a hand sample of the fault surface. The measured point cloud is edited to restrict the data to patches of well-defined fault and remove extraneous objects such as bushes and cracks. The Fourier spectrum of each fault patch is then calculated following the established procedure (for details, see the Data Repository).

The resulting spectra of the topographic profiles of the faults fit a power law function of wavelength, as can be seen from the linear trend on a log-log graph (Fig. 1). The data can be fit by an equation of the form $p(\lambda) = C\,\lambda^{1+2\zeta}$ where C is a constant prefactor, ζ is known as the Hurst or roughness exponent, and λ is the wavelength.

There is a transformation between power spectra density and average asperity height. Given an observation scale, L, the mean asperity height is an integral of the power up to that scale. The power law scaling of the spectra therefore implies power law scaling between roughness and observation scale. In this case, the roughness is related to the observation scale by

$$H = KL^{\zeta}, \quad (1)$$

where H is the average height of asperities at L, and K is a constant prefactor that can be computed from the integration and Parseval's theorem. The resulting value of K is $[C/(2\zeta)]^{1/2}$ (Brodsky et al., 2011).

Surfaces well-described by the power law scaling of Equation 1 with $\zeta = 1$ are known as self-similar. Those with $\zeta \neq 1$ are known as self-affine. Roughness at a given length scale is then captured by the aspect ratio H/L. Surfaces with steep topography have high aspect ratios; smooth

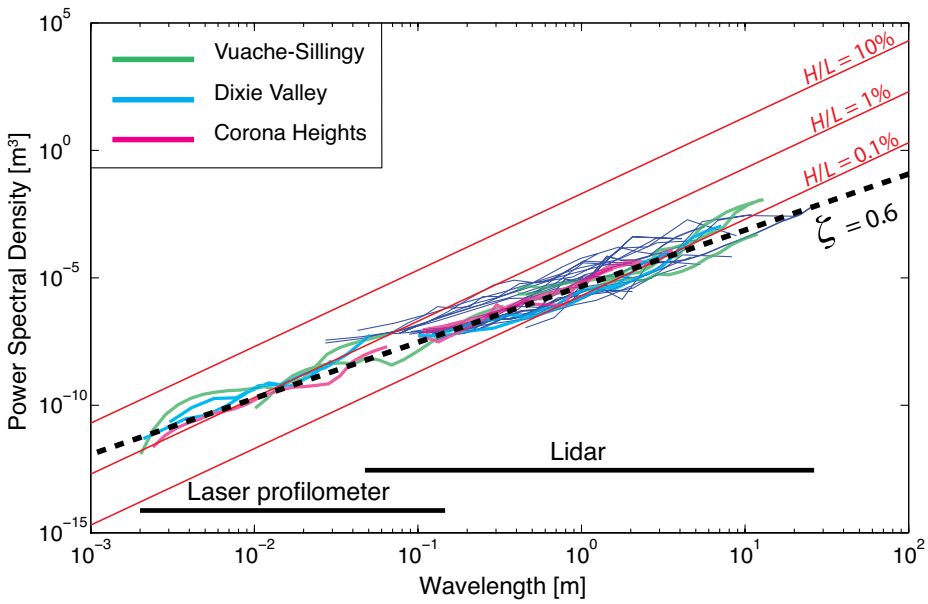

Figure 1. Compilation of extant roughness data for power spectral density (adapted from Brodsky et al., 2011; Candela et al., 2012; Kirkpatrick and Brodsky, 2014). *H/L*— roughness aspect ratio; ζ—Hurst exponent (see text). Blue spectra are the Fourier power spectra observed on the 22 faults in Table DR1 (see footnote 1). We highlight spectra of three individual faults (Vuache-Sillingy, France; Dixie Valley, Nevada, USA; Corona Heights, California, USA) that are connected between lidar and laser profilometer scale.

[1]GSA Data Repository item 2016005, documentation of faults, is available online at www.geosociety.org/pubs/ft2016.htm, or on request from editing@geosociety.org or Documents Secretary, GSA, P.O. Box 9140, Boulder, CO 80301, USA.

surfaces have low ratios. As can be seen from Equation 1, the aspect ratio scales as $KL^{\zeta-1}$.

In this paper we review the major features of fault roughness that have been observed to date with a focus on the aspect ratio H/L and its scale dependence to interpret the data. The scaling of the aspect ratio is used to infer the dependence of rock strength. The interpretation is explored for a particular fault where we find geological evidence of failure at multiple scales.

MAJOR FEATURES OF FAULT ROUGHNESS DATA

Measurements of fault surfaces exhibit a surprisingly narrow range of roughness (Fig. 1). In the slip-parallel direction, the range of aspect ratio H/L is 0.07% to 0.5% for profiles of 1 m length, i.e., $L = 1$ m. In other words, the prefactor K is limited to ~7×10^{-4} to 5×10^{-3} $m^{-\zeta}$. (Note that the units of K for a self-affine fault are dependent on the Hurst exponent, as shown.) This observation is surprising given the wide range of lithologies, deformation histories, and exhumation depths considered (see Table DR1). The observation suggests a statistical robustness to the field measurements that allows extrapolation to faults in general and therefore application of the field measurements to models of dynamic rupture and strong motion generation (Dieterich and Smith, 2009; Dunham et al., 2011; Fang and Dunham, 2013).

Such a restricted range of roughness measurements could potentially be attributed to sampling biases. Field-scale surfaces were only identified for scanning if they were relatively smooth, i.e., $H/L << 1$. In particular, we selected single segments of a fault for scanning and avoided discrete stepovers. At the field scale, measurements of smoother, machined surfaces establish that roughness could be measured with a range error of 3–4 mm (Brodsky et al., 2011). At the laboratory scale, the measurement of a planar reference surface indicates that the roughness range error is 1 µm (Candela et al., 2012). For outcrops with structure at the scale of meters, and for hand samples with structure at the scale of millimeters, the minimum measureable aspect ratio in both cases is ~10^{-4}. The limits on K imposed by the measurement restrictions are therefore 10^{-4} to 1 $m^{-\zeta}$. The observed range of 7×10^{-4} to 5×10^{-3} $m^{-\zeta}$ is thus more restricted than the resolvable range.

We see in Figure 1 that at smaller scales, each fault is rougher with higher aspect ratios than at large scales. Some early measurements of fault roughness were well-fit by self-similar power laws with constant aspect ratio (Hurst exponent $\zeta = 1$) (Power and Tullis, 1991). Modern data have reduced the variance of the power spectral estimation by massive averaging, and the resulting higher precision spectra show rougher topography at smaller scales. This feature is captured by a Hurst exponent $\zeta < 1$. For example, the slip-parallel profiles yield $\zeta = 0.6$, which results in the aspect ratio H/L scaling as $L^{-0.4}$. Variations in the prefactor K obscure the trend for the composite data set and therefore the exponent can only be meaningfully fit for a single fault at a time. The increasing roughness at small scales is clear even in the raw topography data, which show that faults typically are rougher at the centimeter scale than the meter scale (Fig. 2; Fig. DR1).

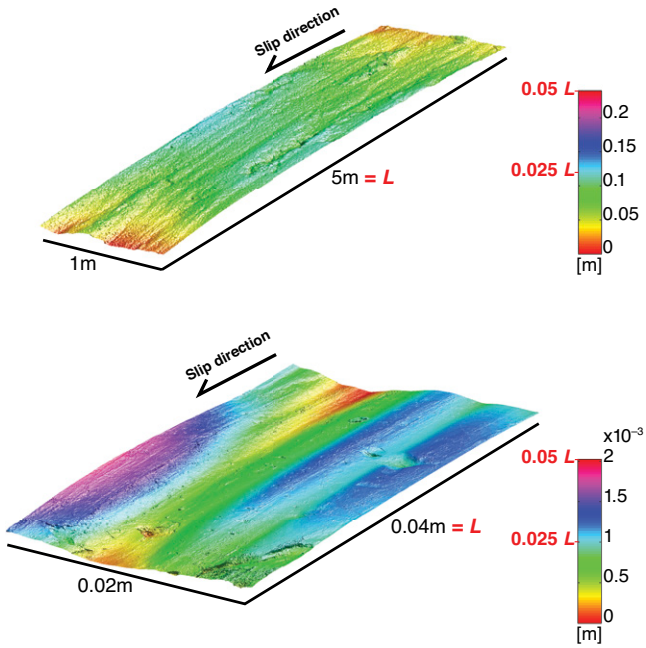

Figure 2. Fault patches of the Corona Heights fault (California, USA) demonstrating the scale-dependent roughness behavior in the spatial domain. For each fault patch (lidar at the top and laser profilometer at the bottom), the maximum of the color scale (red) is set to be equal 0.05 *L*, the measured patch length in the slip direction. At the lidar scale (top), the roughness magnitude reaches only ~0.01 *L*, whereas at the laser profilometer scale, it reaches ~0.05 *L*.

The limited data available suggest that this scaling persists over length scales from 10^{-3} to 10^{1} m in the slip-parallel direction. This consistency is quite surprising given the wide variety of processes known to operate at diverse scales. As we discuss here, surfaces are influenced by processes including intragranular fracture, abrasional grooving, linkage of segments, and constructional mullions. One might expect that each process would produce distinct, characteristic roughness behavior at the scales at which it dominates; the straight line on a log-log plot of roughness as a function of length scale suggests otherwise.

In summary, the major features of our data compilation that need to be explained are the restricted range of roughness (aspect ratio) values, and increased roughness at smaller scales. In this paper we seek a unified physical explanation of these features by examining the influence of material strength on fault roughness.

STRAINS DURING SLIP LIMITED BY STRENGTH

When two rough surfaces slide against each other under a high load, the asperities must deform (Fig. 3). Two uncorrelated rough surfaces slipping parallel to a mean fault plane require asperities to either flatten or fail to accommodate the motion. The complete flattening of the contact requires a deformation of the surface asperity of length L normal to the surface by its height H. By definition, the shear strain ε in the plane normal to contacting surface is the displacement normal to the contacting surface divided by the length over which this displacement is accommodated. This definition implies that ε is proportional to H/L. This general scaling is confirmed by rigorous solutions such as that for elastic deformation of a spherical (Hertzian) contact (for description, see the Data Repository).

The shear strain may not be accommodated elastically. For intact, flawless materials, the theoretical limit of strength is 10% of the Young's modulus (Griffith, 1921; Lawn, 1993). For typical materials with shear modulus equal to approximately half the Young's modulus, the corresponding limiting shear strain is ~10%. In the presence of flaws, stress concentrations cause brittle failure at strains that are orders of

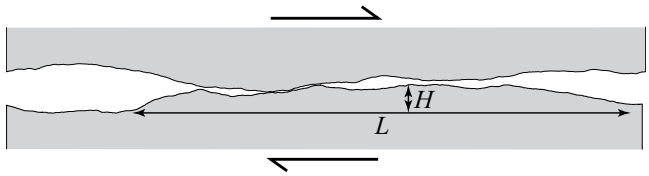

Figure 3. Asperity interaction as two rough surfaces collide. The elastic strain required for the surfaces to slide past each other is on the order of the aspect ratio (*H*/*L*; see text). If this strain exceeds the elastic limit, then failure occurs and the asperities are truncated.

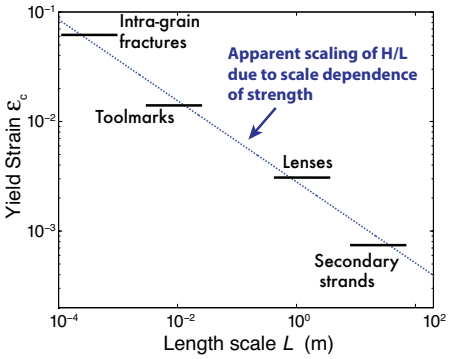

Figure 4. Schematic illustration of the connection between strength and roughness. Dashed line is a fit to values of roughness aspect ratio (*H*/*L*) measured from a terrestrial lidar scan of the exposed Corona Heights fault (California, USA) ($K = 2.8 \times 10^{-3}$ $m^{-\zeta}$) and $\zeta = 0.63$ (ζ is the Hurst exponent) (Kirkpatrick and Brodsky, 2014). Horizontal lines schematically illustrate potential inelastic yielding processes that would each result in a value of failure strain, ε_c. Specific values of ε_c are for illustration purposes only. The array of yielding processes results in the observed roughness.

magnitude lower, and 1% is a typical extreme limit at high strain rates for centimeter-scale laboratory samples (Doan and Billi, 2011). Plastic failure may be preferred over brittle failure when the requisite strain for plastic failure is lower than the brittle threshold (Brace and Kohlstedt, 1980). Whether plastic or brittle failure occurs depends on a variety of factors, including scale, asperity size, lithology, temperature, and strain rate. In any case, strains >1% cannot be sustained elastically (Means, 1976).

The details of the inelastic failure and deformation mechanisms may vary considerably, but the fact that yielding occurs is robust and is required by elastic shakedown (Melan, 1938; Williams, 2005). As a fault slides, the strain, and therefore the aspect ratio of an asperity that can be sustained during sliding is limited by a maximum strain ε_c. In general, ε_c could potentially be a function of the same complicating factors influencing the inelastic processes. Because we observe a variation of *H*/*L* most systematically with scale, we focus on ε_c as a function of scale.

As the fault slips, it roughens through formation of constructional features, damage to the surface, dynamic branching, and deformation (Brodsky et al., 2011). The roughening pushes the surface to the failure limit where the geometry of the surface is limited by the strength of the material, and

$$H / L \sim \varepsilon_c(L). \quad (2)$$

In Figure 1, *H*/*L* in the slip-parallel direction increases with decreasing scale and is proportional to $L^{-0.4}$. The implication is that the yield strain ε_c during surface formation follows the same scaling, i.e.,

$$\varepsilon_c \propto L^{-0.4}. \quad (3)$$

Equation 3 is a key result of this work. At the elastic limit, the yield strain corresponds to an elastic stress $\sigma_c = 2G\varepsilon_c$, where G is the shear modulus. The quantity σ_c is a measure of the strength of the rock at the deformation rates and conditions of fault slip. We suggest that the fault roughness measurements provide a constraint on the scale-dependent strength. Scale-dependent strength has long been recognized in rocks (Jaeger and Cook, 1976), but inferring the rock strength from the surface roughness is a new approach.

Equation 3 conforms to the expectation that rocks are weaker at large scales. A common explanation for decreasing strength with scale is that larger scales encompass larger flaws. The statistical effects of a distribution of flaws on strength are captured by the Weibull distribution (Paterson and Wong, 2005). Based on the probability of intersecting a weak flaw, the critical stress for failure is related to volume, V, by $\sigma_c \sim V^{-1/m}$, which is equivalent to $\sigma_c \sim L^{-3/m}$ where m is the Weibull exponent (Weibull, 1951; Jaeger and Cook, 1976). For the observed Hurst exponent of 0.6, the resultant value of m is 7.5, which is within the typical range of Weibull distribution parameters (Jaeger and Cook, 1976). Alternative explanations for scale-dependent strength can be constrained similarly by the roughness data.

Any more detailed interpretation of the strength requires an identification of the exact yield process. For example, if the yielding is by brittle failure of shear cracks, then the stress required for failure is determined by the fracture energy and the flaw length as

$$\sigma_c \propto (2\gamma / c_f)^{1/2}, \quad (4)$$

where γ is the fracture energy and c_f is maximum length of a flaw in the asperity (Lawn, 1993). If the size of the largest available flaw increases linearly with scale, σ_c decreases as the square root of scale (Scholz, 2002). Dislocation density can introduce a similar scale dependence within the plastic flow regime if conditions dictate that plasticity is the preferred failure mechanism (Greer and De Hosson, 2011). In either case, strength varies as the square root of grain size in a phenomenon known as Hall-Petch scaling (Petch, 1953). The field scale inferred scaling of strength as $\sim L^{-0.4}$ in Equation 3 differs only slightly from Petch-Hall scaling, but here we are examining the dependence of strength on asperity scale rather than grain size.

Note that the strength we infer from the surface roughness is a property of the bulk rock. Frictional strength on the interface is a consequence of the failure within and between individual asperities. Predicting the aggregate solid frictional stress requires solving for the entire interacting system of asperities. Such a complete description of friction is clearly beyond the scope of this work; we confine ourselves here to the implications for scale-dependent bulk rock strength.

Alternative explanations for the roughness scaling of fracture surfaces have focused on either percolation of microbranches or the elastic wavefield around propagating tensile (mode I) cracks (J.P. Bouchaud et al., 1993; Hull, 1999; E. Bouchaud et al., 2002). These studies show that mode I cracks consistently have Hurst exponents of 0.8. In contrast, fault slip surfaces are shear cracks (mode II or III) and the observed Hurst exponent here is 0.6 in the slip direction. This difference is not surprising as the stress field locally is different than in the crack tip region of a tensile fracture. In addition, slip surfaces are sheared against the opposite side for large distances, as evidenced by offset orders of magnitude larger than can be easily explained by single ruptures (Chester et al., 1993; Brodsky et al., 2011). All of these features of the shear slip surfaces motivate us to interpret the fault surfaces based on sliding wear rather than tensile failure.

CASE STUDY: CORONA HEIGHTS FAULT

To make our proposal concrete, we examine how the scale-dependent failure manifests on a particular fault. We recently reported on evidence for inelastic failure of fault surfaces at field scales (Kirkpatrick and Brodsky, 2014); we interpreted the lack of deflection of slickenlines around mullions on the fault surface as evidence of inelastic yielding of meter-scale lenses of cataclasite during sliding. A yield strain of ~1% was sufficient to explain the data.

We did not consider scale-dependent yielding in detail in the previous work. The proposed interpretation here is that yielding occurs at all of the scales for which we have measured roughness with a consistent self-affine scaling. In the case of the Corona Heights fault (California, USA), the observed Hurst exponent is 0.63 over scales of 10^{-3} to 10^{1} m, which implies that the yield strain, and therefore strength, is proportional to $L^{-0.47}$ (Fig. 4).

Geological evidence exists for failure at all of these scales on the Corona Heights fault. At the millimeter scale on this fault, grains fracture (Kirkpatrick et al., 2013). At the centimeter scale, there are tool marks. At the meter scale, the nondeflection of the slickenlines indicates failure of the topographically high lenses. At the several meters scale, branching fractures define the edges of the lenses.

All of these structural features are common on many faults. This case study where both the roughness data and geological information are available simply highlights the direct manifestation of failure at multiple scales.

CONCLUSIONS AND IMPLICATIONS

The identification of failure processes on the Corona Heights fault is encouraging, and a more quantitative comparison with strength at various scales would clearly be desirable. However, independent measures of scale-dependent strength in situ in the crust are few. That knowledge gap motivates the current effort. The inferences from roughness presented here may in turn motivate development of new techniques to measure the strengths now illustrated schematically in Figure 4.

The scaling of strength proposed here poses a problem at small scales where H/L appears to increase without bound, and at large scales where the implication is that faults become infinitely weak (Fig. 4). The power law scaling can only exist within a limited range of scales. At small scales, a limit could be imposed by the absolute strength of the intact, flawless rock (Griffith, 1921; Lee et al., 2008). Investigations into the ultrastrength of small-scale samples also suggest alternative failure modes at small scales (Zhu et al., 2009). At the scale at which the failure mode or constitutive law changes, the change in the physical origin of the scale-dependent strength should result in a change in the Hurst exponent. At large scales, a limit to the wear mechanisms could be imposed by the total offset on the fault (Bistacchi et al., 2011). Beyond the limit, other processes, such as fault linkage, may dominate (Segall and Pollard, 1983).

If correct, the recording of strength by fault roughness has both macroscopic and microscopic implications. Macroscopically, the establishment of a physical mechanism controlling roughness sets the stage for extrapolation of the fault measurements to depths and faults inaccessible to field investigation. For example, if high temperature at depth weakens the rocks, in the absence of any other complications, the fault should be smoother.

Microscopically, the observed scale dependence of roughness implies yielding of asperities at all scales. This is qualitatively different from micromechanical models of friction that define a scale below which asperities yield to determine the real area of contact (Bowden and Tabor, 1950). The adjustment of the real area of contact is the fundamental process that makes friction proportional to normal stress and the coefficient of friction a well-defined quantity. A careful examination of the real area of contact on rough surfaces with scale-dependent yielding may be necessary before applying laboratory coefficients of friction to natural systems.

ACKNOWLEDGMENTS

We thank C. Thom, D. Goldsby, A. Sagy, D. Turcotte, and F. Renard for helpful comments on drafts of this manuscript. We also thank C. Scholz and two anonymous reviewers for further improvements. We gratefully acknowledge support of the Gordon and Betty Moore Foundation.

REFERENCES CITED

Bistacchi, A., Griffith, W.A., Smith, S.A.F., di Toro, G., Jones, R., and Nielsen, S., 2011, Fault roughness at seismogenic depths from LiDAR and photogrammetric analysis: Pure and Applied Geophysics, v. 168, p. 2345–2363, doi:10.1007/s00024-011-0301-7.

Bouchaud, E., Bouchaud, J.P., Fisher, D.S., Ramanathan, S., and Rice, J.R., 2002, Can crack front waves explain the roughness of cracks?: Journal of the Mechanics and Physics of Solids, v. 50, p. 1703–1725, doi:10.1016/S0022-5096(01)00137-5.

Bouchaud, J.P., Bouchaud, E., Lapasset, G., and Planès, J., 1993, Models of fractal cracks: Physical Review Letters, v. 71, p. 2240–2243, doi:10.1103/PhysRevLett.71.2240.

Bowden, F.P., and Tabor, D., 1950, The friction and lubrication of solids: Oxford, UK, Oxford University Press, 186 p.

Brace, W., and Kohlstedt, D., 1980, Limits on lithospheric stress imposed by laboratory experiments: Journal of Geophysical Research, v. 85, NB11, p. 6248–6252, doi:10.1029/JB085iB11p06248.

Brodsky, E.E., Gilchrist, J.J., Sagy, A., and Collettini, C., 2011, Faults smooth gradually as a function of slip: Earth and Planetary Science Letters, v. 302, p. 185–193, doi:10.1016/j.epsl.2010.12.010.

Brown, S.R., and Scholz, C.H., 1985, Broad bandwidth study of the topography of natural rock surfaces: Journal of Geophysical Research, v. 90, no. B14, p. 2575–2582, doi:10.1029/JB090iB14p12575.

Candela, T., Renard, F., Klinger, Y., Mair, K., Schmittbuhl, J., and Brodsky, E.E., 2012, Roughness of fault surfaces over nine decades of length scales: Journal of Geophysical Research, v. 117, B08409, doi:10.1029/2011JB009041.

Chester, F., Evans, J., and Biegel, R., 1993, Internal structure and weakening mechanisms of the San Andreas fault: Journal of Geophysical Research, v. 98, p. 771–786, doi:10.1029/92JB01866.

Dieterich, J.H., and Smith, D.E., 2009, Nonplanar faults: Mechanics of slip and off-fault damage: Pure and Applied Geophysics, v. 166, p. 1799–1815, doi:10.1007/s00024-009-0517-y.

Doan, M.-L., and Billi, A., 2011, High strain rate damage of Carrara marble: Geophysical Research Letters, v. 38, L19302, doi:10.1029/2011GL049169.

Dunham, E.M., Belanger, D., Cong, L., and Kozdon, J.E., 2011, Earthquake ruptures with strongly rate-weakening friction and off-fault plasticity, Part 2: Nonplanar faults: Seismological Society of America Bulletin, v. 101, p. 2308–2322, doi:10.1785/0120100076.

Fang, Z., and Dunham, E.M., 2013, Additional shear resistance from fault roughness and stress levels on geometrically complex faults: Journal of Geophysical Research, v. 118, p. 3642–3654, doi:10.1002/jgrb.50262.

Greer, J.R., and De Hosson, J.T.M., 2011, Plasticity in small-sized metallic systems: Intrinsic versus extrinsic size effect: Progress in Materials Science, v. 56, p. 654–724, doi:10.1016/j.pmatsci.2011.01.005.

Griffith, A.A., 1921, The phenomena of rupture and flow in solids: Royal Society of London Philosophical Transactions, ser. A, v. 221, p. 163–198, doi:10.1098/rsta.1921.0006.

Hull, D., 1999, Fractography: Observing and interpreting fracture surface topography: Cambridge, UK, Cambridge University Press, 386 p.

Jaeger, J.C., and Cook, N.G.W., 1976, Fundamentals of rock mechanics: London, Chapman and Hall, 585 p.

Kirkpatrick, J.D., and Brodsky, E.E., 2014, Slickenline orientations as a record of fault rock rheology: Earth and Planetary Science Letters, v. 408, p. 24–34, doi:10.1016/j.epsl.2014.09.040.

Kirkpatrick, J.D., Rowe, C.D., White, J.C., and Brodsky, E.E., 2013, Silica gel formation during fault slip: Evidence from the rock record: Geology, v. 41, p. 1015–1018, doi:10.1130/G34483.1.

Lawn, B., 1993, Fracture of brittle solids (second edition): Cambridge, UK, Cambridge University Press, 400 p., doi:10.1017/CBO9780511623127.

Lee, C., Wei, X., Kysar, J.W., and Hone, J., 2008, Measurement of the elastic properties and intrinsic strength of monolayer graphene: Science, v. 321, p. 385–388, doi:10.1126/science.1157996.

Lee, J.J., and Bruhn, R.L., 1996, Structural anisotropy of normal fault surfaces: Journal of Structural Geology, v. 18, p. 1043–1059, doi:10.1016/0191-8141(96)00022-3.

Lyell, C., 1871, The student's elements of geology: New York, Harper & Brothers, 650 p., doi:10.1680/tseog.52581.

Means, W.D., 1976, Stress and strain, basic concepts of continuum mechanics for geologists: New York, Springer-Verlag, 339 p.

Melan, E., 1938, Zur Plastizität des räumlichen Kontinuums: Ingenieur-Archiv, v. 9, p. 116–126, doi:10.1007/BF02084409.

Paterson, M.S., and Wong, T.-F., 2005, Experimental rock deformation—The brittle field: Berlin, Springer, 348 p.

Petch, N.J., 1953, The cleavage strength of polycrystals: Journal of the Iron and Steel Institute, v. 174, p. 25–28.

Power, W., and Tullis, T., 1991, Euclidean and fractal models for the description of rock surface roughness: Journal of Geophysical Research, v. 96, no. B1, p. 415–424, doi:10.1029/90JB02107.

Power, W., Tullis, T., and Weeks, J., 1988, Roughness and wear during brittle faulting: Journal of Geophysical Research, v. 93, no. B12, p. 15,268–15,278, doi:10.1029/JB093iB12p15268.

Renard, F., Voisin, C., Marsan, D., and Schmittbuhl, J., 2006, High resolution 3D laser scanner measurements of a strike-slip fault quantify its morphological anisotropy at all scales: Geophysical Research Letters, v. 33, L04305, doi:10.1029/2005GL025038.

Sagy, A., Brodsky, E.E., and Axen, G., 2007, Evolution of fault-surface roughness with slip: Geology, v. 35, p. 283–286, doi:10.1130/G23235A.1.

Scholz, C.H., 2002, The mechanics of earthquakes and faulting: Cambridge, UK, Cambridge University Press, 504 p, doi:10.1017/CBO9780511818516.

Segall, P., and Pollard, D.D., 1983, Nucleation and growth of strike slip faults in granite: Journal of Geophysical Research, v. 88, p. 555–568, doi:10.1029/JB088iB01p00555.

Weibull, W., 1951, A statistical distribution function of wide applicability: Journal of Applied Mechanics, v. 18, p. 293–297.

Williams, J., 2005, Engineering tribology: Cambridge, UK, Cambridge University Press, doi:10.1017/CBO9780511805905.

Zhu, T., Li, J., Ogata, S., and Yip, S., 2009, Mechanics of ultra-strength materials: MRS Bulletin, v. 34, p. 167–172, doi:10.1557/mrs2009.47.

Manuscript received 29 July 2015
Revised manuscript received 22 October 2015
Manuscript accepted 25 October 2015

Printed in USA